Ozone-Regenerable Mesoporous Zeolite Y Pellets Synthesized Hydrothermally And Modified With Fe^{3+}/Mn^{2+} For Dye Adsorption

Vo Tran Minh Khoa[1], Nguyen Manh Khang[1], Huynh Diem Nhung[1], Van Chi Khen[1], Pham Thi Tuyet[1,2], and Nguyen Quang Long[1,2*]

[1] *Faculty of Chemical Engineering, Ho Chi Minh City University of Technology (HCMUT), 268 Ly Thuong Kiet Street, Dien Hong ward, Ho Chi Minh City, Vietnam*
[2] *Vietnam National University Ho Chi Minh City (VNU-HCM), Ho Chi Minh City, Vietnam*
[*] *Corresponding author. E-mail: nqlong@hcmut.edu.vn*

Received: March 30, 2026; Accepted: July 13, 2026

The design of regenerable adsorbents is critical for sustainable wastewater treatment. Mesoporous zeolite Y pellets were synthesized through hydrothermal dealumination-desilication and modified by Fe^{3+} and Mn^{2+} ion exchange. Characterization confirmed preservation of the FAU framework, while BET analysis showed enlarged external surface areas of 102 m^2/g for hierarchical Y, 81 m^2/g for VM80, and 72 m^2/g for Fe-VM80. Column experiments indicated that methylene blue adsorption followed pseudo-first-order kinetics. Ozone regeneration outperformed the Fenton process, shortening treatment times to 1.5 h for Mn-VM80 and 1 h for Fe-VM80 while maintaining higher cyclic stability. The combination of hierarchical porosity, pelletization, and Fe/Mn modification enabled efficient adsorption-desorption cycling. These ozone-regenerable mesoporous zeolite Y pellets show strong potential as scalable and sustainable adsorbents for dye removal.

Keywords: Mesoporous zeolite Y; MB adsorption; Regeneration; Ozonation; hydrothermal synthesis

http://dx.doi.org/10.6180/jase.202612_35.004

1. Introduction

Synthetic dyes are widely used because of their easy synthesis, strong coloration, and high stability, which can be applied in various sectors, including the textile, pulp mill, dye synthesis, food, printing, and plastic [1]; however, their extensive discharge has become a major source of water pollution [2]. Organic compositions are the primary components of the synthetic dyes, and these compounds have a hard time degrading in the natural environment, and threaten different life forms due to their high chemical oxygen demand of water and the toxicity to humans [2, 3]. Cationic dyes are generally considered more hazardous than anionic dyes due to their higher interaction with negatively charged biological membranes [4, 5]. Methylene blue (MB) is one of the most representative cationic dyes that is widely used in textile, pharmaceutical, garment, and hair-coloring industries [6]. Its high stability and widespread use make MB persistent in the environment and resistant to degradation. As a potentially toxic and carcinogenic pollutant, prolonged exposure may cause anemia, vomiting, eye irritation, and mental confusion [3, 4].

Dye removal from wastewater has been achieved using various methods, such as ion exchange, membrane filtration, oxidation, electrolysis, photocatalysis, and enzymatic treatment [7–10]. Of these, the adsorption technique is gaining traction due to its simple design and operation, high efficiency, and harmlessness to the treated water [3]. Zeolites are porous aluminosilicate materials possess high porosity, surface area, and adjustable pore size and negatively charged frameworks which are conducive to adsorbents for cationic dye removal [11–14]. Among them, zeolite Y(FAU- type), is popular for its high stability under harsh

working conditions [15–17]. However, its inherent microporous structure can impose diffusion limitations, restricting access to active sites and thereby reducing adsorption efficiency for larger dye molecules [18]. Although hierarchical zeolites can overcome this limitation by enhancing mass transfer, their synthesis often involves complex and costly procedures, restricting large-scale applications [16, 19, 20]. Consequently, hierarchical porous materials with simple synthesis routes are needed for efficient wastewater treatment.

In this study, microporous zeolite Y was converted into a hierarchical structure via a two-step hydrothermal dealumination–desilication process and pelletized for methylene blue removal in a fixed-bed column. This work integrates hierarchical structuring, pelletization, Fe^{3+}/Mn^{2+} modification, and regeneration within a single continuous-flow system. Adsorption behavior was analyzed using kinetic and isotherm models. The resulting materials exhibited improved mass transfer, operational stability, and regeneration performance, demonstrating their potential for scalable wastewater treatment.

2. Material and methods

2.1. Preparation of mesoporous zeolite Y pellets

Mesoporous zeolite Y(MeY) was synthesized by hydrothermal method based on a previous study [21] with some modifications. Sodium hydroxide (NaOH), citric acid ($C_6H_8O_7$), iron (III) chloride hexahydrate ($FeCl_3 \cdot 6H_2O$), and manganese (II) nitrate ($Mn(NO_3)_2$) were used in the material synthesis. Firstly, 25 g of zeolite Y were dispersed in 300 mL of 0.1 mol/L citric acid and stirred at room temperature for 1 h. The suspension was then subjected to hydrothermal treatment at 100 °C for 4 h in a Teflon-lined autoclave. Subsequently, 230 mL of 0.2 mol/LNaOH solution was added, followed by a second hydrothermal treatment at 65 °C for 1 h. The product was centrifuged, filtered, washed, and dried at 80 °C to obtain hierarchical zeolite Y.

For pelletization, the obtained powder was homogeneously mixed with bentonite at the ratios listed in Table 1. A small amount of distilled water was added to improve adhesion. The mixture was extruded using a 20 mL syringe to form rod-like structures and air-dried. The materials were then processed on a rotating disk at 9 Hz for 30 min to form pellets, followed by drying at 100 °C and calcination for 4 h to obtain hierarchical zeolite pellets (VM).

2.2. Ion-exchange modification

For the ion-exchange modification, 3.0 g of VM were immersed in 200 mL of 0.15 mol/L $FeCl_3 \cdot 6H_2O$ solution and stirred at room temperature for 12 h to obtain Fe-based materials. For Mn-based materials, 3.0 g of VM were added to a mixed solution containing 150 mL of 0.15 mol/LMn $(NO_3)_2$ and 50 mL of 0.8 mol/LH_2O_2, followed by stirring at room temperature for 12 h to ensure homogenization. Subsequently, the resulting materials were vacuum-filtered, thoroughly washed, and dried at 60°C to obtain the Fe- and Mn-exchanged hierarchical zeolite pellets, denoted as Fe-VM80 and Mn-VM80, respectively.

Table 1. Composition of hierarchical zeolite pellets.

Sample	Zeolite Y/Bentonite ratio	Calcination temperature
VM95	95-5	x
VM90	90-10	x
VM85	85-15	x
VM80-550	80-20	550
VM80-600	80-20	600

2.3. Adsorption study

In this study, methylene blue (MB) was removed from an aqueous solution through pellet-based adsorption, followed by regeneration using advanced oxidation processes. Briefly, 3 g of the adsorbent pellets were packed into a column (35 cm in height and 1.5 cm in inner diameter) equipped with a supporting layer. The packed pellets occupied a volume of approximately 4.9 mL , corresponding to a packing density of 0.61 g/mL. A 50 ppm MB solution (pH $\sim$ 6) was continuously fed through the column in a downward-flow mode at a flow rate of 15 mL/s. After 3 h of adsorption, the exhausted adsorbent was regenerated using either ozone-assisted oxidation or the Fenton process. A schematic illustration of the methylene blue treatment system is presented in Fig. 1.

$$\log(q_e) = \log(K_F) + \frac{1}{n}\log(C_e) \tag{1}$$

$$\frac{C_e}{q_e} = \frac{C_e}{q_{\max}} + \frac{1}{q_{\max} K_L} \tag{2}$$

where: qe and qmax: saturated and maximum adsorption capacity $(mg.g^{-1})$, Ce; the saturated concentration of MB (ppm), KL: Langmuir constant, n: empirical constant.

Adsorption kinetics are pivotal in investigating how fast an adsorbent can be applied to treat wastewater. Therefore, pseudo-first-order (PFO) and pseudo-second-order (PSO) models are utilized in this study [6,20]. The linear equations for the two kinetic models are:

$$\ln(q_e - q_t) = \ln(q_e) - k_1 t \tag{3}$$

$$\frac{t}{q_t} = \frac{1}{k_2 \times q_e^2} + \frac{t}{q_e} \tag{4}$$

where: qt and qe: kinetic and saturated adsorption capacity ($mg.g^{-1}$), Ce; the saturated concentration of MB (ppm), k_1 and k_2 : adsorption rate constant of PFO and PSO models, respectively, t: adsorption time (min).

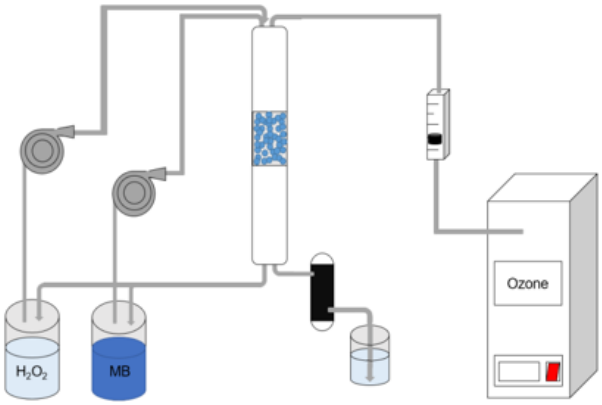

Fig. 1. Column-based system design for methylene blue treatment.

Regarding the ozone-assisted regeneration process, ozone at a concentration of 0.175 mg/L was introduced into the column at a flow rate of 2 L/min. At the predetermined time intervals, the adsorbent colour was observed to assess the MB degradation capacity to determine the optimal regeneration time for later cycles. For the Fenton process, the H_2O_2 stream of 0.5 mol/L flowed through the column until the pH reached 3. The observation of the adsorbent colour was also conducted to evaluate the MB degradation capacity.

3. Results and discussion

3.1. Pellet Formation

The pelletization behavior of hierarchical zeolite Y was investigated using bentonite as a binder at zeolite-to-bentonite mass ratios of 95:5, 90:10, 85:15, and 80:20 [22]. The obtained pellets generally exhibited a circular shape with diameters ranging from 2 to 4 mm. Low binder contents resulted in poor extrusion and fragile pellets, whereas increasing the bentonite content improved pellet formation. The 80:20 ratio produced the highest pellet yield (∼80%) with well-defined spherical pellets (Table 2) and was therefore selected for subsequent experiments.

3.2. Characterization

The XRD patterns of hierarchical zeolite Y powders and pellet samples are presented in Fig. 2a. The characteristic diffraction peaks of zeolite Y (JCPDS 43-0168) within the 2θ ranges of $6° - 16°$ and $23° - 32°$ were observed in all synthesized samples, indicating that the fundamental zeolite framework was largely preserved after pore modification and ion-exchange treatments. However, the hierarchical samples exhibited lower diffraction intensities than the standard zeolite Y, suggesting reduced crystallinity due to hydrothermal desilication, which may induce structural disorder or partial framework collapse upon silicon removal [23]. The Fe-VM80 and Mn-VM80 pellets contained 34.01 and 30.10 g/kg of Fe and Mn, corresponding to mass fractions of 3.401% and 3.01%, respectively (Fig. 2b).

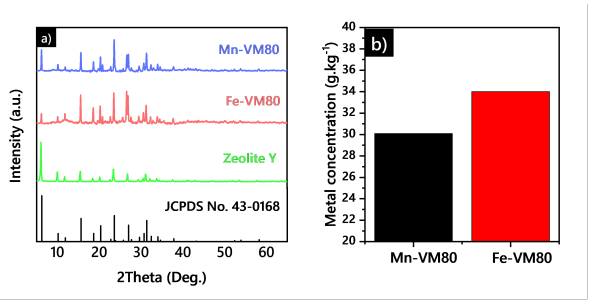

Fig. 2. Crystallinity and ion-exchanged concentration.

Fig. 3 illustrates the nitrogen adsorption-desorption isotherms of zeolite Y, hierarchical zeolite Y, VM80, and Fe-VM80. Zeolite Y exhibited a type I isotherm (IUPAC), characteristic of microporous materials [24], whereas the synthesized samples displayed type IV isotherms with hysteresis loops, indicating of the presence of mesopores [18] which confirming the successful pore modification of zeolite Y through dealumination and desilication. Pelletized samples exhibited an additional peak around 20, and their textural properties are summarized in Fig. 3. Dealumination and desilication reduced the specific surface area (S_{BET}) but markedly increased the external surface area ($S_{external}$), indicating partial transformation of micropores into mesopores. Accordingly, the external surface area increased by approximately 2-3 times after modification. Pelletization further reduced S_{BET} from 505.7 to 390.1 m^2/g, likely due to binder-induced pore blockage and increased particle size [13, 22]. Moreover, the mesopore volume fraction increased from 14% in the parent zeolite to 35% in hierarchical zeolite Y and approximately 50% in VM80 and Fe-VM80. The slightly lower total pore volume of Fe-VM80 compared with VM80 may be attributed to partial pore blockage by Fe^{3+} ions during ion exchange.

3.3. Study of isotherm and kinetic MB adsorption

3.3.1. Isotherm Study

As shown in Fig. 4c, adsorption equilibrium ($5,77 mg/g$) was reached within 180 min at the highest MB concentration (250 ppm); therefore, this contact time was used for all

Table 2. Influence of bentonite binder content on pellet formation.

Zeolite/ bentonite ratio	Suspension property	Pellet formation	Yield
95:5	Low viscosity	Few fragile pellets	Low
90:10	Slightly viscous	Limited pellets	Low
85:15	Sticky	Well-formed pellets	Moderate
80:20	Highly viscous	Uniform spherical pellets	80%

Table 3. Analysis of surface area and pore characteristics of various samples.

Parameters	Sample			
	Zeolite Y	Hierarchical zeolite Y	VM80	Fe-VM80
S_{BET} (m^2/g)	735.9	505.7	390.1	296.8
$S_{external}$ (m^2/g)	33.6	101.8	81.0	72.0
S_{micro} (m^2/g)	702.3	403.9	309.0	224.7
V_{total} (cm^3/g)	0.33	0.26	0.27	0.17
V_{meso} (cm^3/g)	0.04	0.09	0.15	0.08
V_{micro} (cm^3/g)	0.29	0.17	0.12	0.09

Table 4. Isotherm parameters and coefficients of Freundlich and Langmuir.

Freundlich			Langmuir		
$K_F(mg/g)$	n	R^2	$K_L(L/mg)$	q_{max} (mg/g)	R^2
1.204	3.22	0.9357	0.03	7.18	0.9544

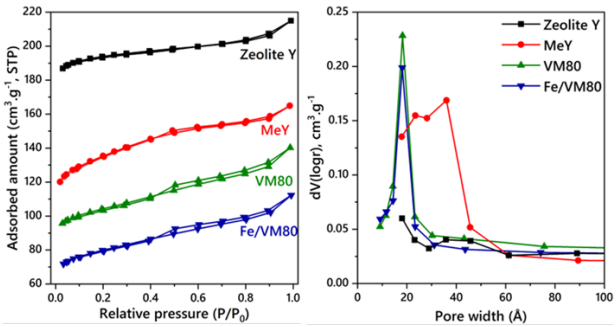

Fig. 3. Surface area and pore characteristics of zeolites and modified hierarchical zeolites.

subsequent experiments. Figures 4d, 4e, and Table 4 reveal that both isotherm models fit the experimental data well. However, MB adsorption followed the Langmuir model more closely, with a correlation coefficient (R^2) of 0.9544. This model assumes a homogeneous distribution of adsorption sites and monolayer adsorption on the adsorbent surface [25]. According to the Langmuir model, the maximum adsorption capacity of MB was 7.18 mg/g. This can be explained by the results of N_2 adsorption-desorption isotherms. The decrease in S_{BET} value as the powder samples were transformed into pellet shape then the active sites were reduced. In addition, based on BJH results, the average pore diameter of shaped pellets were fell below 20 Amstrong while the dimension of MB molecules were recorded as 13.72 × 9.7 Amstrong [26]. Consequently, this reduction in pore size of pellets as compared to powder samples, which can be attributed to pore blocking of bentonite binder, made it difficult for MB adsorption process as the dimension of molecules and pores were comparable.

Although this value is not particularly high, it represents monolayer saturation at equilibrium, where the surface of the adsorbent is fully covered by MB molecules [27]. Additionally, by applying the Langmuir constant (KL) and the entire range of initial concentrations (C0) into Eq. (3)), the calculated RL values fall within the range of 0–1, indicating that MB adsorption is a favorable process. Regarding the Freundlich model, which describes a heterogeneous adsorption system, the correlation coefficient was 0.9357. The 1/n value was within the range of 0–1, which also reflects a favorable adsorption process and a relatively high affinity of MB for the adsorbent surface [28].

3.3.2. *Kinetic Study*

In this study, an experiment was conducted by allowing an aqueous solution of 50 ppm methylene blue (MB) to flow through a column containing 1 gram of VM80, and the adsorption capacity was recorded over time, as shown in Fig. 5a. The pseudo-first order (PFO) and pseudo-second order (PSO) kinetic models were fitted to the experimental contact time data, as illustrated in Fig. 5b, with the corresponding parameters listed in Table 5. It is noteworthy that the PFO model provided the best fit, with a correlation coefficient (R^2) of 0.9993 , indicating that the MB uptake rate is directly proportional to the difference between the satura-

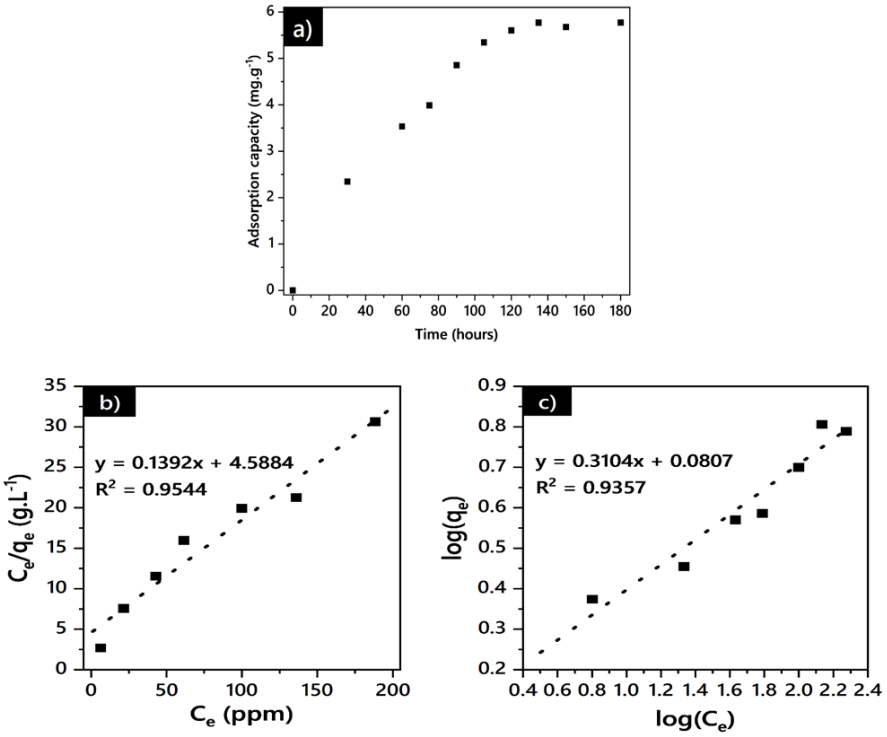

Fig. 4. (a) Kinetic investigation for maximum adsorption capacity, (b,c) Langmuir and the Freundlich model.

tion concentration and the amount adsorbed by VM80 over time [27]. In addition, the calculated equilibrium adsorption capacity (qe) closely matched the experimental value (2.85mg/g vs. 2.848mg/g). In contrast, the PSO model showed a poorer fit $(R^2 = 0.9186)$, and the estimated qe value (5.56mg/g) deviated significantly from the experimental result (2.848mg/g).

3.4. Regeneration study

3.4.1. Ozonation

The regeneration results of hierarchical zeolite Y and ion-modified hierarchical zeolite pellets are presented in Fig. 6a,b,c and Table 6. Overall, ion-exchange modification improved regeneration efficiency and reduced regeneration time. Fe-VM80 and Mn-VM80 showed smaller losses in adsorption capacity, retaining about 50% efficiency after the first regeneration, followed by only $\sim$ 5% decreases over the next two cycles. MB degradation is mainly attributed to the direct reaction between ozone (O_3) and MB molecules, consistent with the findings of B. Jaramillo-Sierra [29]. Fe^{3+} ion exchange slightly reduced the adsorption efficiency compared with VM80, consistent with the lower pore volume observed from N_2 adsorption-desorption analysis. However, adsorption efficiencies remained at 35% and 32% after regeneration, indicating improved stability and lower performance loss. This enhancement is attributed to Fe^{3+} catalytic sites, which promote ozone decomposition into highly reactive hydroxyl radicals. These radicals can interact with target contaminants adsorbed on the pellet surface, facilitating their degradation [30]. Kishimoto et al. demonstrated that Fe^{3+} can generate hydroxyl radicals ($^{\bullet}OH$) through Eq. (5), in addition to the self-decomposition pathway of ozone. The hydroxyl radicals formed play a key role in the degradation of organic compounds [31], thereby accelerating the regeneration process.

$$Fe^{3+} + O_3 + (H_2O) \rightarrow FeO^{2+} + OH^{\bullet} + O_2 + H^{+} \quad (5)$$

Among the tested samples, Mn-VM80 exhibited the lowest MB adsorption capacity, with an initial adsorption efficiency of only 30% in the first regeneration cycle. However, its regeneration performance was comparable to that of fe-Mons, requiring only 1.5 h for regeneration and showing a minimal decrease in adsorption efficiency ($\sim$3%) after multiple cycles.

3.4.2. Fenton - like process

As shown in Table 6, the Fenton process required a significantly longer time for sample regeneration compared to the ozonation method. Specifically, the regeneration times for VM80, Mn-VM80, and Fe-VM80 were 12, 10, and 6 h,

Table 5. Kinetic parameters of the PFO and PSO models.

Pseudo-first order			Pseudo-second order		
k_1	q_e(mg/g)	R^2	k_2	$q_e(mg/g)$	R^2
0.012	2.85	0.9993	0.001	5.53	0.9168

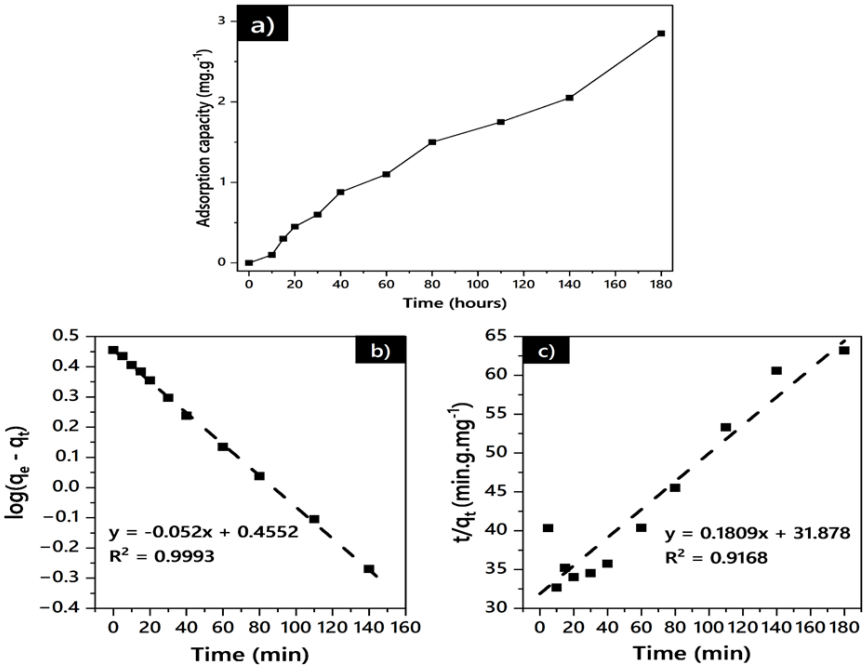

Fig. 5. (a) Kinetic adsorption capacity, (b-c) PFO and PSO kinetic models.

Table 6. Regeneration time for ozonation and Fenton processes.

Sample	Regeneration time (hours)	
	Ozonation	Fenton-like
VM80	2	12
Fe-VM80	1.5	6
Mn-VM80	1.5	10

respectively. This decreasing trend is attributed to the enhancement of the heterogeneous Fenton process through the introduction of Fe^{3+} and Mn^{2+} ions. In the study by H.G. Quynh et al [32] the degradation process using only H_2O_2 resulted in a low MB removal efficiency, while the Fenton process employing Fe/ZA catalyst achieved significantly higher degradation performance under the same time frame. The study also proposed a reaction mechanism in which the presence of Fe^{3+} contributed to the generation of $^{\bullet}HO_2$ radicals, as illustrated in Eqs. (6) and (7). Regarding Mn^{2+} ions, through the Fenton-like process, it has been reported as an effective catalyst for the degradation of organic compounds under acidic conditions (pH 3), with the free radical generation mechanism described in Eq. (8) [33].

$$H_2O_2 + Fe^{3+} \rightarrow H^+ + FeOOH^{2+} \quad (6)$$

$$FeOOH^{2+} \rightarrow^{\bullet} HO_2 + Fe^{2+} \quad (7)$$

$$Mn^{2+} + H_2O_2 \rightarrow Mn^{3+} +^{\bullet} OH + OH^- \quad (8)$$

With respect to adsorption efficiency, as illustrated in Fig. 6d and Table 7, a similar trend was observed in comparison to the ozonation process, where all samples exhibited a gradual decline in efficiency across regeneration cycles, accompanied by a widening deficiency gap. The VM80 sample showed an 18% loss in adsorption efficiency, compared with only 10% after ozone regeneration. Fe^{3+} - and Mn^{2+}-modified samples exhibited higher stability during the first two cycles, with efficiency losses below 5%. In later cycles, adsorption efficiency declined to 25.8% and 19.4%, respectively, although the overall decrease remained lower than that of VM80. The improved early-cycle performance is attributed to Fe^{3+} and Mn^{2+} catalyzing Fenton-like reactions. As these active species were gradually depleted, MB degradation weakened from the third cycle onward,

Table 7. Regeneration results for Fenton-like process.

	Regeneration cycle	VM80	Fe-VM80	Mn-VM80
Adsorption efficiency (%)	Cycle 1	48.78	40.46	32.08
	Cycle 2	42.48	39.18	28.52
	Cycle 3	37.96	31.56	22.36
	Cycle 4	30.44	25.80	19.40

consistent with the low residual metal content determined by AAS.

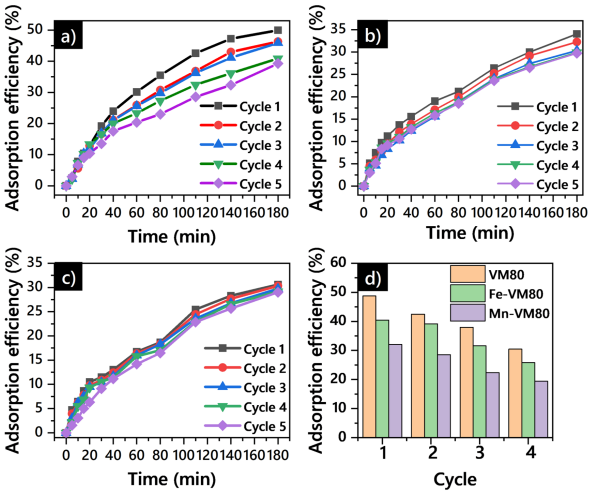

Fig. 6. Adsorption efficiency through the ozone-assisted regeneration method of (a) VM80, (b) Fe-VM80, and (c) Mn-VM80; (d) Regeneration under H2O2 of various samples.

4. Conclusions

Mesoporous zeolite Y was successfully synthesized via hydrothermal dealumination-desilication and shaped into mechanically stable pellets for fixed-bed applications. The modified zeolite preserved the FAU framework while developing hierarchical porosity. Experimental results confirmed effective adsorption performance, and ozone regeneration outperformed the Fenton process by providing faster regeneration and better cyclic stability. Fe^{3+} and Mn^{2+} incorporation enhanced catalytic degradation, sustaining adsorption efficiency. This integrated strategy offers regenerable zeolite-based adsorbents with strong potential for scalable wastewater treatment. For future work, additional characterization techniques, including XPS, FTIR, SEM-EDS, and TEM, should be employed to elucidate the oxidation states, bonding environments, and spatial distribution of Fe and Mn species within the zeolite framework. Furthermore, during the regeneration process, TOC and COD analyses, together with Fe and Mn leaching measurements, should be performed to provide deeper insight into the regeneration mechanism and the long-term stability of the catalyst.

Acknowledgements

This research is funded by Vietnam National University Ho Chi Minh City (VNU-HCM) under a project within the framework of the Program titled "Strengthening the capacity for education and basic scientific research integrated with strategic technologies at VNU-HCM, aiming to achieve advanced standards comparable to regional and global levels during the 2025-2030 period, with a vision toward 2045"", under grant number: CB2025-20-11. We acknowledge Ho Chi Minh City University of Technology (HCMUT), VNU-HCM, for supporting this study.

Disclosure statement

All authors declare no financial or non-financial competing interests.

References

[1] D. Zhao, W. Zhang, C. Chen, and X. Wang, (2013) *"Adsorption of Methyl Orange Dye Onto Multiwalled Carbon Nanotubes"* **Procedia Environmental Sciences *18***: 890–895. DOI: 10.1016/j.proenv.2013.04.120.

[2] L. Wu, X. Liu, G. Lv, R. Zhu, L. Tian, M. Liu, Y. Li, W. Rao, T. Liu, and L. Liao, (2021) *"Study on the adsorption properties of methyl orange by natural one-dimensional nano-mineral materials with different structures"* **Scientific Reports *11***: 10640. DOI: 10.1038/s41598-021-90235-1.

[3] S. Rahmani, B. Zeynizadeh, and S. Karami, (2020) *"Removal of cationic methylene blue dye using magnetic and anionic-cationic modified montmorillonite: kinetic, isotherm and thermodynamic studies"* **Applied Clay Science *184***: 105391. DOI: 10.1016/j.clay.2019.105391.

[4] J. Fito, M. Abewaa, A. Mengistu, K. Angassa, A. D. Ambaye, W. Moyo, and T. Nkambule, (2023) *"Adsorption of methylene blue from textile industrial wastewater using activated carbon developed from Rumex abyssinicus plant"* **Scientific Reports *13***: 5427. DOI: 10.1038/s41598-023-32341-w.

[5] N. M. Thuan, N. T. M. Linh, N. T. T. Phuong, N. T. H. Duong, N. M. Hung, P. T. Tuyet, N. Van Dung, and N. Q. Long, (2024) *"Ethanolamine-modified zeolite – Chitosan beads as new adsorbents for carbon dioxide capture and crystal violet removal"* **Case Studies in Chemical and Environmental Engineering *10***: 100917. DOI: 10.1016/j.cscee.2024.100917.

[6] F. Poorsajadi, M. H. Sayadi, M. Hajiani, and M. R. Rezaei, (2022) *"Synthesis of CuO/Bi2O3 nanocomposite for efficient and recycling photodegradation of methylene blue dye"* **International Journal of Environmental Analytical Chemistry *102***: 7165–7178. DOI: 10.1080/03067319.2020.1826464.

[7] C. Kathing and G. Saini, (2022) *"A Review of Various Treatment Methods for the Removal of Dyes from Textile Effluent"* **Recent Progress in Materials *4***: 1–15. DOI: 10.21926/rpm.2204028.

[8] C. Langa, N. Mabuba, L. M. Mahlaule-Glory, D. E. Motaung, Z. Tetana, and N. C. Hintsho-Mbita, (2026) *"Enhanced photocatalytic degradation of dyes and pharmaceutical pollutants using Fe/TiO2-carbon nanospheres from Sutherlandia Frutescence"* **International Journal of Environmental Analytical Chemistry *106***: 790–820. DOI: 10.1080/03067319.2025.2524833.

[9] L. Mouni, L. Belkhiri, J.-C. Bollinger, A. Bouzaza, A. Assadi, A. Tirri, F. Dahmoune, K. Madani, and H. Remini, (2018) *"Removal of Methylene Blue from aqueous solutions by adsorption on Kaolin: Kinetic and equilibrium studies"* **Applied Clay Science *153***: 38–45. DOI: 10.1016/j.clay.2017.11.034.

[10] G. Bal and A. Thakur, (2022) *"Distinct approaches of removal of dyes from wastewater: A review"* **Materials Today: Proceedings *50***: 1575–1579. DOI: 10.1016/j.matpr.2021.09.119.

[11] K. Rida, S. Bouraoui, and S. Hadnine, (2013) *"Adsorption of methylene blue from aqueous solution by kaolin and zeolite"* **Applied Clay Science *83-84***: 99–105. DOI: 10.1016/j.clay.2013.08.015.

[12] T. P. Le, H. V. T. Luong, H. N. Nguyen, T. K. T. Pham, T. L. Trinh Le, T. B. Q. Tran, and T. N. M. Ngo, (2024) *"Insight into adsorption-desorption of methylene blue in water using zeolite NaY: Kinetic, isotherm and thermodynamic approaches"* **Results in Surfaces and Interfaces *16***: 100281. DOI: 10.1016/j.rsurfi.2024.100281.

[13] N. M. Khang, V. T. Minh Khoa, N. T. Truc Phuong, N. X. Du, N. T. Hoang Duong, N. Van Dung, T. T. Tuyet Mai, and N. Q. Long, (2025) *"Double-xerogel network composite zeolite granules targeting dual-functional fertilizers"* **Case Studies in Chemical and Environmental Engineering *12***: 101253. DOI: 10.1016/j.cscee.2025.101253.

[14] D. M. El-Mekkawi, F. A. Ibrahim, and M. M. Selim, (2016) *"Removal of methylene blue from water using zeolites prepared from Egyptian kaolins collected from different sources"* **Journal of Environmental Chemical Engineering *4***: 1417–1422. DOI: 10.1016/j.jece.2016.01.007.

[15] H. J. Choi, D. Jo, J. G. Min, and S. B. Hong, (2021) *"The Origin of Selective Adsorption of CO2 on Merlinoite Zeolites"* **Angewandte Chemie International Edition *60***: 4307–4314. DOI: 10.1002/anie.202012953.

[16] B. Reiprich, T. Weissenberger, W. Schwieger, and A. Inayat, (2020) *"Layer-like FAU-type zeolites: A comparative view on different preparation routes"* **Frontiers of Chemical Science and Engineering *14***: 127–142. DOI: 10.1007/s11705-019-1883-3.

[17] M. Narimani, M. Gonbadi, and M. M. Zerafat, (2025) *"Methylene blue adsorption on Y-zeolite as a nano-porous adsorbent: equilibrium and kinetic studies"* **International Journal of Environmental Analytical Chemistry *105***: 5369–5389. DOI: 10.1080/03067319.2024.2392632.

[18] N. T. T. Phuong, N. M. Thuan, N. T. M. Linh, N. Van Dung, N. T. H. Duong, and N. Q. Long, (2024) *"Effects of organic acids on microwave-assisted leaching for mesopore generation in FAU zeolite"* **Applied Physics A *130***: 734. DOI: 10.1007/s00339-024-07879-9.

[19] X. Yin, Z. Li, S. Wang, N. Chu, J. Yang, and J. Wang, (2015) *"Hydrothermal synthesis of hierarchical zeolite T aggregates using tetramethylammonium hydroxide as single template"* **Microporous and Mesoporous Materials *201***: 247–257. DOI: 10.1016/j.micromeso.2014.09.018.

[20] T. T. P. Nguyen, Q. T. Le Nguyen, H. H. Lam, V. D. Nguyen, H. D. Ngo Tran, and N. Quang Long, (2022) *"Enhancement Of CO2 Adsorption By Introducing Mesopores Into FAU Zeolite Using Acid-Base Leaching"* **Journal of Applied Science and Engineering *26***: 791–798. DOI: 10.6180/jase.202306_26(6).0005.

[21] R. Zhang, P. Zhong, H. Arandiyan, Y. Guan, J. Liu, N. Wang, Y. Jiao, and X. Fan, (2020) *"Using ultrasound to improve the sequential post-synthesis modification method for making mesoporous Y zeolites"* **Frontiers of Chemical Science and Engineering *14***: 275–287. DOI: 10.1007/s11705-019-1905-1.

[22] Z. Asgar Pour, M. Abduljawad, Y. Alassmy, L. Cardon, P. Steenberge, and K. Sebakhy, (2023) *"A Comparative Review of Binder-Containing Extrusion and Alternative Shaping Techniques for Structuring of Zeolites into Different Geometrical Bodies"* **Catalysts *13***: 656. DOI: 10.3390/catal13040656.

[23] Q. G. Ho, L. T. Bui, P. T. T. Nguyen, D. T. H. Ngo, and L. Q. Nguyen, (2023) *"Modification of ZSM-5 Catalyst Using Microwave-Assisted and Thermal Methods: Characterizations and n-Heptane Cracking Activity"* **Chemical Engineering Transactions *106***: 907–912. DOI: 10.3303/CET23106152.

[24] L. K. Anh, T. T. Q. Nhu, L. T. T. Hien, N. T. Thong, N. T. T. Phuong, N. Van Dung, N. T. H. Duong, and N. Q. Long, (2025) *"Highly mesoporous X zeolites synthesized by microwave-assisted sequential dealumination-desilication for methylene blue adsorption and toluene photocatalytic removal"* **International Journal of Environmental Science and Technology *22***: 12763–12780. DOI: 10.1007/s13762-025-06436-y.

[25] T. Huang, M. Yan, K. He, Z. Huang, G. Zeng, A. Chen, M. Peng, H. Li, L. Yuan, and G. Chen, (2019) *"Efficient removal of methylene blue from aqueous solutions using magnetic graphene oxide modified zeolite"* **Journal of Colloid and Interface Science *543***: 43–51. DOI: 10.1016/j.jcis.2019.02.030.

[26] J.-C. Bollinger, E. C. Lima, L. Mouni, S. Salvestrini, and H. N. Tran, (2025) *"Molecular properties of methylene blue, a common probe in sorption and degradation studies: a review"* **Environmental Chemistry Letters *23***: 1403–1424. DOI: 10.1007/s10311-025-01856-1.

[27] K. Y. Hor, J. M. C. Chee, M. N. Chong, B. Jin, C. Saint, P. E. Poh, and R. Aryal, (2016) *"Evaluation of physicochemical methods in enhancing the adsorption performance of natural zeolite as low-cost adsorbent of methylene blue dye from wastewater"* **Journal of Cleaner Production *118***: 197–209. DOI: 10.1016/j.jclepro.2016.01.056.

[28] R. Han, J. Zhang, P. Han, Y. Wang, Z. Zhao, and M. Tang, (2009) *"Study of equilibrium, kinetic and thermodynamic parameters about methylene blue adsorption onto natural zeolite"* **Chemical Engineering Journal *145***: 496–504. DOI: 10.1016/j.cej.2008.05.003.

[29] B. Jaramillo-Sierra, A. Mercado-Cabrera, A. Arias, R. Peña-Eguiluz, R. López-Callejas, B. Rodríguez, and R. Alvarado, (2019) *"Methylene blue degradation assessment by advance oxidation methods"* **Journal of Applied Research and Technology *17***: DOI: 10.22201/icat.16656423.2019.17.3.809.

[30] A. Ikhlaq, R. Fatima, U. Qazi, R. Javaid, A. Akram, S. Ibn Shamsah, and F. Qi, (2021) *"Combined Iron-Loaded Zeolites and Ozone-Based Process for the Purification of Drinking Water in a Novel Hybrid Reactor: Removal of Faecal Coliforms and Arsenic"* **Catalysts *11***: 373. DOI: 10.3390/catal11030373.

[31] Z. U. H. Khan, N. S. Gul, S. Sabahat, J. Sun, K. Tahir, N. S. Shah, N. Muhammad, A. Rahim, M. Imran, J. Iqbal, T. M. Khan, S. Khasim, U. Farooq, and J. Wu, (2023) *"Removal of organic pollutants through hydroxyl radical-based advanced oxidation processes"* **Ecotoxicology and Environmental Safety *267***: 115564. DOI: 10.1016/j.ecoenv.2023.115564.

[32] H. G. Quynh, H. V. Thanh, N. T. T. Phuong, N. P. T. Duy, L. H. Hung, N. V. Dung, N. T. H. Duong, and N. Q. Long, (2023) *"Rapid removal of methylene blue by a heterogeneous photo-Fenton process using economical and simple-synthesized magnetite–zeolite composite"* **Environmental Technology & Innovation *31***: 103155. DOI: 10.1016/j.eti.2023.103155.

[33] A. P. Sarmento, A. C. Borges, A. T. de Matos, and L. L. Romualdo, (2016) *"Phenol degradation by Fenton-like process"* **Environmental Science and Pollution Research *23***: 18429–18438. DOI: 10.1007/s11356-016-6835-6.